Suppression of longitudinal modes in two-sectioned, coupled-cavity GaAs/(Al,Ga)As terahertz quantum-cascade lasers

M. Giehler,[a] H. Kostial, R. Hey, and H. T. Grahn
Paul-Drude-Institut für Festkörperelektronik, Hausvogteiplatz 5-7, 10117 Berlin, Germany

(Received 24 July 2007; accepted 13 September 2007; published online 15 October 2007)

The spectra of two-sectioned, coupled-cavity (TSCC) terahertz quantum-cascade lasers exhibit a number of longitudinal modes, which are periodically suppressed due to interference effects. The number of suppressed modes is equal to the ratio of the lengths of the two subcavities. At maximum laser output, the mode suppression disappears due to optical saturation, and a switching between TSCC and single-cavity-like mode features appears for certain delays between the current pulses through the individual subcavities. A transfer-matrix approach reproduces the mode spacings very well, but predicts a smaller modulation of the mode heights and does not describe the observed mode switching. © *2007 American Institute of Physics*. [DOI: 10.1063/1.2794008]

A two-sectioned, coupled-cavity (TSCC) laser consists of two optically coupled subcavities of lengths L_1 and L_3 separated by a gap of width L_2, as schematically shown in Fig. 1. For interband TSCC lasers, monitoring of longitudinal laser modes, wavelength tuning, chaotic behavior, or self-pulsation of lasing have been studied.[1–4] For intersubband TSCC lasers, Hvozdara *et al.*[5] have demonstrated single-mode operation in midinfrared (MIR) quantum-cascade lasers (QCLs). We investigate the modulation of the longitudinal modes in terahertz TSCC QCLs by varying the lengths and currents in the two subcavities and analyze the observed behavior on the basis of a transfer-matrix (T-matrix) approach. We focus on a system with $L_2 \approx 1$ μm, which is much smaller than the corresponding laser wavelength $\lambda \approx 100$ μm of terahertz QCLs. This is in contrast to MIR QCLs ($\lambda \approx 9$ μm) as discussed in Ref. 5, where $L_2 \approx \lambda$.

The investigated terahertz GaAs/(Al,Ga)As QCLs are based on the design introduced by Barbieri *et al.*[6] The air gap is formed by cleaving the laser ridge. Typical longitudinal-mode spectra as a function of frequency ν are shown in Figs. 2(a) and 3(b) for sample A with $L_3/L_1=1.2$ and sample B with $L_3/L_1=3.7$ (spectrum for 1.4 A), respectively, indicated by thick lines. The longitudinal modes of terahertz TSCC QCLs exhibit two main features. First, all modes exhibit a slight deviation from an equidistant mode spacing, independently of the current levels I_j through the two subcavities $j=1$ and 3. The average value of the mode spacing $\Delta\nu_{\mathrm{all}}=c/[2n_{\mathrm{eff}}(L_1+L_3)]$, where $n_{\mathrm{eff}}=3.71$ denotes the effective refractive index and c the speed of light, is equal to the one of an equivalent single-cavity laser. This observation indicates that in terahertz TSCC QCLs the laser light penetrates from one subcavity into the other and vice versa, because $L_2 \ll \lambda$. In contrast, the observed mode-spacing characteristic in MIR TSCC QCLs (not shown here) depends for appropriate values of I_1 and I_3 either on L_1 or L_3 alone. This different behavior of MIR with respect to terahertz devices demonstrate that the laser radiation can be predominantly located in one subcavity. Second, for a total current $I=I_1+I_3<I_c$, where I_c denotes the current value for maximum laser output, the mode heights of terahertz TSCC QCLs exhibit a pronounced modulation. This behavior is in contrast to the one observed in single-cavity QCLs, where all modes have the same intensity, except for features due to the gain and loss spectra as well as random inhomogeneities in the laser ridge. In TSCC spectra, a number of L_3/L_1 (assuming without loss of generality that $L_3>L_1$) modes are suppressed, which are referred to in the following as minor modes. These minor modes appear between modes of high intensity, which are called major modes. The spacing between the major modes is determined by $\Delta\nu_{\mathrm{maj}}=\Delta\nu_{\mathrm{all}}(1+L_3/L_1)=c/(2n_{\mathrm{eff}}L_1)$. Because for sample A $L_3/L_1=1.2$, almost every major mode is followed by a minor mode as can be seen in Fig. 2(a), and we obtain $\Delta\nu_{\mathrm{all}}=0.0088$ THz and $\Delta\nu_{\mathrm{maj}}=0.0194$ THz, which agree well with the measured data. According to the ratio $L_3/L_1=3.7$ for sample B, three to four modes are suppressed as visible in Fig. 3(b) for the spectra labeled 1–1.4 A, and we obtain $\Delta\nu_{\mathrm{all}}=0.0073$ THz and $\Delta\nu_{\mathrm{maj}}=0.0343$ THz.

In order to analyze the experimental results, we apply a T-matrix approach. The partial waves propagating in the medium j are described by $A_j \exp\{\pm i\Phi_j z\}$, where $\Phi_j=2\pi n_{\mathrm{eff}}\tilde{\nu}+i(\alpha_j-\Gamma g_j)/2$, $\tilde{\nu}$ denotes the wavenumber, α_j the internal optical losses due to energy dissipation, and Γg_j the modal gain. We assume that each photon emission caused by an intersubband transition is not affected by the total local laser field. Then α_j, Γg_j, and n_{eff} are constant. However, each emitted partial wave is influenced by its self-interference within the total TSCC resonator, which can be taken into account in the following way:

$$\begin{pmatrix} A_0 \\ B_0 \end{pmatrix} = \left(\prod_{j=1}^{3} D_{j-1,j} P_j \right) D_{3,4} \begin{pmatrix} A_4' \\ B_4' \end{pmatrix} = \mathbf{T} \begin{pmatrix} A_4' \\ B_4' \end{pmatrix}. \tag{1}$$

The amplitudes A_j and B_j and their primed counterparts are indicated in Fig. 1. The general dependence of the interface

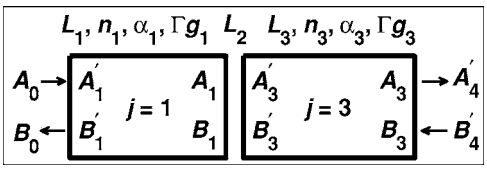

FIG. 1. Geometry of the TSCC laser. A_j and B_j denote the amplitude of the partial wave propagating to the right and left, respectively, on the left (unprimed) or right side (primed) of the interface $j-1,j$.

[a]Electronic mail: giehler@pdi-berlin.de

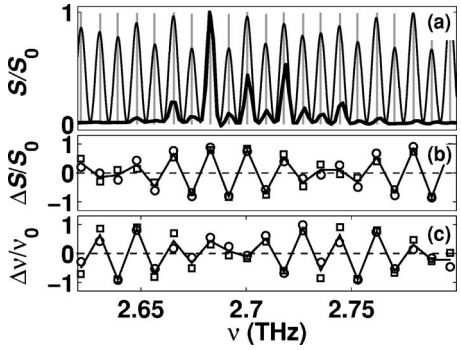

FIG. 2. (a) Normalized longitudinal-mode spectrum (thick line) of sample A ($L_3/L_1=1.2$, $L_3+L_1=4610\ \mu$m) at 8 K for $I_3+I_1=1.24$ A ($I_c=1.6$ A), pulse width 200 ns, repetition rate 5 kHz, and a spectral resolution of 0.0035 THz. The vertical gray bars mark the calculated eigenfrequencies using Eq. (3). The spectrum indicated by the thin line was calculated using Eq. (4). (b) Calculated normalized modulation degree of the mode heights and (c) mode spacings. The squares and circles in (b) and (c) refer to calculated results obtained using Eqs. (3) and (4), respectively.

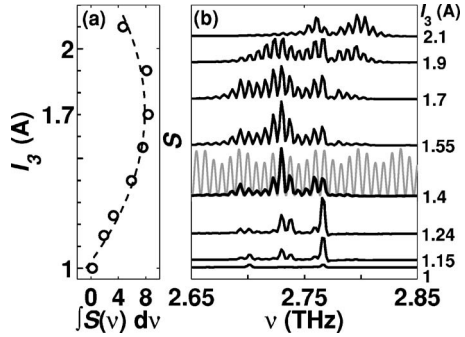

FIG. 3. (a) Integrated intensity and (b) longitudinal-mode spectra of sample B ($L_3/L_1=3.7$, $L_3+L_1=5360\ \mu$m) for $I_1=0.6$ A ($I_c=2.3$ A) and different values of I_3. The gray spectrum was calculated using Eq. (4). The dashed line in (a) is a guide to the eye.

matrix $D_{j-1,j}$ as well as propagation matrix P_j and the reflection coefficient $r_{j-1,j}$ on Φ_j are given in Ref. 7. According to Eq. (1) and the condition that there is no incoming light from outside the laser ($A_0=B_4'=0$), the complex eigenwavenumbers $\hat{\tilde{\nu}}_m$ of the longitudinal modes are determined by

$$\begin{aligned} T_{11}(\hat{\tilde{\nu}}_m) = (1 + r_{01}r_{12}\exp\{i2\hat{\Phi}_1\})(1 + r_{23}r_{34}\exp\{i2\hat{\Phi}_3\}) \\ + [(r_{12} + r_{01}\exp\{i2\hat{\Phi}_1\})(r_{23} + r_{34})\exp\{i2(\hat{\Phi}_2 \\ + \hat{\Phi}_3)\}] = 0, \end{aligned} \tag{2}$$

where $\hat{\Phi}_j=\Phi_j L_j+\pi m$ and m denotes the mode index. The measurable real wavenumbers of the laser modes are described by $\tilde{\nu}_m=\mathrm{Re}\{\hat{\tilde{\nu}}_m\}$, whereas $\mathrm{Im}\{\hat{\tilde{\nu}}_m\}$ is a measure of the attenuation of the modes. On the right-hand side of Eq. (2), the first (and also the second) bracket of the first term alone would describe the eigenwavenumbers of a single-cavity laser,

$$\hat{\tilde{\nu}}_m = \frac{-i}{4\pi n_{\mathrm{eff}}}\left[\frac{1}{L_1}\ln\left(\frac{-1}{r_{01}r_{12}}\right) + \alpha_1 - \Gamma g_1\right] + \frac{m}{2n_{\mathrm{eff}}L_1}. \tag{3}$$

For a resonator without waveguide losses and gain ($\alpha_1=0$ and $\Gamma g_1=0$), Eq. (3) shows that the imaginary part of the eigenwavenumber is a measure for the mirror losses. Waveguide losses and modal gain as well as the threshold condition can be described only by taking into account an imaginary part in the refractive index ($\alpha_1\neq 0$ and $\Gamma g_1\neq 0$). From Eq. (3), we obtain for the mode wavenumbers $\tilde{\nu}_m=m/(2n_{\mathrm{eff}}L_1)$. For TSCC QCLs, the meaning of $\hat{\tilde{\nu}}_m$ remains the same. However, $\mathrm{Re}\{\hat{\tilde{\nu}}_m\}$ and $\mathrm{Im}\{\hat{\tilde{\nu}}_m\}$ are coupled with each other [second term in Eq. (2)], and the constructive and destructive interference of each partial wave during its round trip in the TSCC resonator cause a periodic modulation of the mode heights as well as a slight modulation of the mode spacings around $\Delta\nu_{\mathrm{all}}$. The eigenwavenumbers $\hat{\tilde{\nu}}_m$ for TSCC QCLs are more difficult to write in a similar form as Eq. (3). Therefore, we plot the numerical solution of Eq. (2) for sample A in Fig. 2(a) as gray vertical bars using n_{eff} for both subcavities. The frequencies of the bars are determined from $\tilde{\nu}_m=\mathrm{Re}\{\hat{\tilde{\nu}}_m\}$, whereas the heights of the bars are proportional to $-1/\mathrm{Im}\{\hat{\tilde{\nu}}_m\}$. S_0 denotes a normalization constant. In Fig. 2(a), the $\tilde{\nu}_m$ data were shifted by a small, for all modes constant value in order to fit a calculated major mode to the strongest measured one. Figure 2(a) demonstrates that the calculated spacings agree well with the measured ones. However, the determined modulation degree of the mode heights $\langle(S_{\mathrm{major}}-S_{\mathrm{minor}})/(S_{\mathrm{major}}+S_{\mathrm{minor}})\rangle\approx 1.5\%$ is much smaller than the measured value of 62%. Therefore, we analyze the longitudinal modes of terahertz TSCC QCLs also in terms of the so-called spectral function $P(\tilde{\nu})$. We define $P(\tilde{\nu})$ for a resonator without gain and waveguide losses in the following way:

$$P(\tilde{\nu}) = |T_{22} + r_{10}T_{21} + r_{34}T_{12} - r_{10}r_{34}T_{11}|^2. \tag{4}$$

Here, $P(\tilde{\nu})$ is equal to the denominator of Eq. (6.9) in Ref. 8, where Eq. (6.9) was derived for spectra of distributed feedback lasers. The calculated spectrum $P(\tilde{\nu})$ for sample A (B) is shown in Fig. 2(a) [Fig. 3(b)] by the thin (gray) line. The mode heights determined by Eq. (4) exhibit a modulation degree of 12%, which is one order of magnitude larger than the value determined from Eq. (2), but is still clearly smaller than the measured one. Figure 2(b) shows the normalized modulation degree $\Delta S/S_0=(S_m-S_{\mathrm{av}})/(2\gamma S_{\mathrm{av}})$ for sample A calculated from $-1/\mathrm{Im}\{\hat{\tilde{\nu}}_m\}$ and $P(\tilde{\nu})$ indicated by squares and circles, respectively, where S_{av} denotes the average value and γ a scaling factor. The $\Delta S/S_0$ data obtained from Eqs. (2) and (4) exhibit very similar features. The normalized mode spacings $\Delta\tilde{\nu}/\tilde{\nu}_0=(\tilde{\nu}_m-\tilde{\nu}_{\mathrm{av}})/(2\gamma'\tilde{\nu}_{\mathrm{av}})$ for sample A calculated from $\mathrm{Re}\{\hat{\tilde{\nu}}_m\}$ and $P(\tilde{\nu})$ are plotted in Fig. 2(c) indicated by squares and circles, respectively, where γ' denotes a scaling factor. As discussed above and also because of the Kramers-Kronig relation, the $\Delta S/S_0$ and $\Delta\tilde{\nu}/\tilde{\nu}_0$ spectra display similar periodic features. However, the deviation from an equidistant mode spacing is very small, i.e., it is of the order of 1.5×10^{-6} calculated using Eq. (3) and 1×10^{-7} using Eq. (4).

The mode suppression described above can be also influenced by selecting appropriate values of I_1 and I_3. Figures 3(a) and 3(b) show the integrated mode intensity $\int S(\nu)d\nu$ and the spectra, respectively, of sample B for $I_1=0.6$ A and different values of I_3. Figure 3(b) displays that for $I_3<1.55$ A the mode heights exhibit a modulation as described above. However, the mode suppression is strongly reduced near the maximum laser output at $I_3\approx 1.7$ A, where $I_1+I_3\approx I_c\approx 2.3$ A, but reappears for a further increase of I_3.

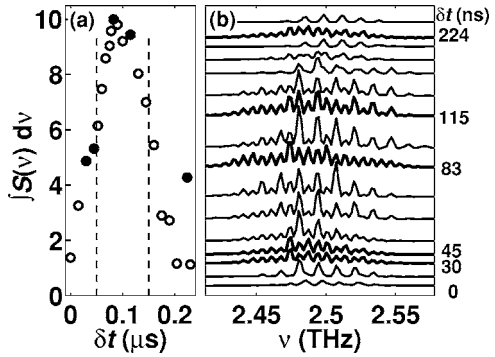

FIG. 4. (a) Integrated intensity vs delay and (b) corresponding mode spectra of sample C ($L_3/L_1=1.03$, $L_3+L_1=5920$ μm, $I_3=I_1=0.7$ A, $I_c=1.9$ A, pulse widths of 100 ns) from bottom to top for $\delta t=0$, 15, 30, 45, 53, 60, 75, 83, 100, 115, 145, 175, 190, 204, 224, and 230 ns as partly indicated on the right-hand side of (b). The dots and circles refer to spectra without and with mode suppression, respectively. The vertical dashed lines in (a) indicate the region of a pulse overlap of more than 50%.

This behavior can be explained by assuming that the maximum laser output is related to a saturation of the laser intensity rather than to a misalignment of the laser levels due to an increasing field strength for $I>I_c$. When the doping density in the injector is increased by a factor of about 2.5, I_c increases from 1.5 to 3 times the threshold current.

Finally, the mode suppression can also be removed by introducing a delay δt between I_1 and I_3 for appropriate values of I_1+I_3 slightly below I_c. Figure 4(a) shows the integrated mode intensity versus δt for sample C ($L_3/L_1=1.03$). The corresponding longitudinal-mode spectra are plotted in Fig. 4(b). With increasing overlap of the current pulses, the intensity increases, and the spectra display a mode suppression with the expected spacing $\Delta\nu_{\mathrm{maj}}=0.014$ THz. However, around $\delta t\approx 40$, 83, 115, and 224 ns, the slope of the intensity versus time delay changes, indicated in Fig. 4(a) by the dots. In the corresponding spectra, shown in Fig. 4(b) as thick lines, all modes appear with almost the same height. The mode suppression is removed, and the spectra are similar to the ones of a single-cavity laser with $\Delta\nu_{\mathrm{all}}=0.0066$ THz. This behavior may be due to dynamical laser effects, which are beyond our approximate model described above.

In summary, the longitudinal modes of TSCC terahertz QCLs exhibit a pronounced modulation of the mode heights due to interference effects, which can be qualitatively described by a *T*-matrix approach. In order to explain the modulation degree as a function of the current and the switching of the mode structure from the one of a TSCC QCL to the one similar to a single-cavity laser, the interplay between photon emission, photon density, and electron population of the intersubband laser levels has to be fully included into the *T*-matrix approach.

The authors would like to thank P. Kleinert and L. Schrottke for valuable discussions.

[1]K. J. Ebeling and L. A. Coldren, J. Appl. Phys. **54**, 2962 (1983).
[2]H. K. Choi, K.-L. Chen, and S. Wang, IEEE J. Quantum Electron. **20**, 385 (1984).
[3]L. A. Coldren, IEEE J. Quantum Electron. **20**, 659 (1984).
[4]M. Radziunas and H.-J. Wünche, Proc. SPIE **4646**, 27 (2002).
[5]L. Hvozdara, A. Lugstein, S. Gianordoli, W. Schrenk, G. Strasser, K. Unterrainer, E. Bertagnolli, and E. Gornik, Appl. Phys. Lett. **77**, 1077 (2000).
[6]S. Barbieri, H. E. Beere, J. Fowler, E. H. Linfield, and D. A. Ritchie, Appl. Phys. Lett. **85**, 1674 (2004).
[7]P. Yeh, *Optical Waves in Layered Media* (Wiley, New York, 1988), p. 102.
[8]G. Morthier, *Handbook of Distributed Feedback Laser Diodes* (Artech House, Inc., Boston, 1997), p. 154.